Lattice Boltzmann Model for Anisotropic Liquid-Solid Phase Transition

W. Miller*
Institut für Kristallzüchtung (IKZ), Max-Born-Strasse 2, 12489 Berlin, Germany

S. Succi and D. Mansutti
Istituto per le Applicazioni del Calcolo (C.N.R.), Viale del Policlinico 137, Rome 00161, Italy
(Received 18 July 2000)

We develop a simple reaction model for the liquid-solid phase transition in the context of the lattice Boltzmann method with enhanced collisions. Calculations for a two-dimensional test problem of Ga melting and for a two-dimensional anisotropic growth of dendrites are presented and commented on.

DOI: 10.1103/PhysRevLett.86.3578 PACS numbers: 64.70.Dv, 44.25.+f, 81.10.Aj

During the last decade lattice gas automata and lattice Boltzmann (LB) methods evolved as powerful tools for the simulation of complex fluid motion and pattern formation. These methods have been applied to many physical problems such as, e.g., phase separation of two immiscible fluids [1]. Only very recently a thermal lattice Boltzmann method has been adapted to the problem of liquid-solid phase transition [2]. De Fabritiis *et al.* used a thermal model with two types of quasiparticles, for liquid and solid phases, respectively. In one dimension, this leads to a 5×5 system of constraints for the reaction terms. Besides being restricted to the one-dimensional case, this model contained a number of empirical parameters and assumptions which cast some doubts on its viability for more realistic studies.

In this Letter, we simplify and extend at a time this previous model by using only one type of quasiparticles and a phase field ϕ, which defines the solid and liquid fraction ($-1 \le \phi \le 1$, where -1 means totally solid and $+1$ totally liquid). The quasiparticles evolve in discrete time t_* on a face-centered hypercubic lattice in which every node $\vec{r}_*$ is surrounded by 24 neighbors i at a distance $|\vec{c}_i| = \sqrt{2}$. These 24 neighbors correspond to the full set of permutations $\vec{c}_i = [\pm 1, \pm 1, \pm 1, \pm 1]$. The distribution N_i of particles with speed $\vec{c}_i$ obeys the following discrete Boltzmann equation [3,4]:

$$N_i(\vec{r}_* + \vec{c}_i, t_* + 1) = N_i(\vec{r}_*, t_*) + F_i^B + F_i^{fs} + F_i^{\mathcal{L}} + \sum_j \mathcal{A}_{ij}[N_j(\vec{r}_*, t_*) - N_j^{\mathrm{eq}}(\vec{r}_*, t_*)]. \quad (1)$$

Here N_j^{eq} is the local equilibrium, which is calculated via an expansion in the lattice gas velocity $\vec{u}(\vec{r}_*, t_*) = \frac{1}{\rho(\vec{r}_*, t_*)} \sum_i \vec{c}_i N_i(\vec{r}_*, t_*)$, where $\rho(\vec{r}_*, t_*) = \sum_i N_i(\vec{r}_*, t_*)$ is the lattice gas density. $\mathcal{A}_{ij}$ is the collision matrix which controls the viscosity ν_* of the lattice fluid via the inverse of its leading nonzero eigenvalue [4]. F_i^B, F_i^{fs}, $F_i^{\mathcal{L}}$ represent the components of the buoyancy force, the drag force, and the heat source, respectively. The buoyancy force is defined via $|\vec{F}^B| = \beta T$, where β is related to the expansion coefficient times gravity acceleration. The drag force and heat source are discussed below. The temperature T is treated as a scalar and identified as the velocity component along the fourth dimension of the FCHC lattice [5,6]. We use the collision matrix given by Massaioli *et al.,* which allows nonunit Prandtl numbers [7,8], extended by a reservoir of rest particles [9]. With a suitable choice of the local equilibrium, the hydrodynamic limit of Eq. (1) is known to reproduce anomaly free Navier-Stokes equations for fluid flow plus the standard transport equation for the temperature field within the Boussinesq approximation.

The phase-field ϕ evolves according to a rate equation:

$$\phi(\vec{r}_*, t_*) = \phi(\vec{r}_*, t_* - 1) + \mathcal{R}(\vec{r}_*, t_*). \quad (2)$$

Since melting/solidification is an activated process, we postulate the following chemical expression for the reaction term $\mathcal{R}(\vec{r}_*, t_*)$:

$$\mathcal{R}(\vec{r}_*, t_*) = f_+ K^+(\vec{r}_*, t_*)[1 - \phi(\vec{r}_*, t_* - 1)] - f_- K^-(\vec{r}_*, t_*)[1 + \phi(\vec{r}_*, t_* - 1)], \quad (3)$$

where f_+, f_- are frequency factors, basically the inverse time scale for solidification/melting, respectively, and K^+, K^- are switch functions controlling the onset of melting/solidification around the critical temperature T_c. The specific form is [$T'(\vec{r}_*, t_*) = T(\vec{r}_*, t_*) - T_c$]:

$$K^{\pm}(\vec{r}_*, t_*) = \frac{1}{2}\left(1 \pm \tanh\{[T'(\vec{r}_*, t_*) \mp T_s]/T_w\}\right), \quad (4)$$

where T_w controls the energy range of the transition and T_s defines two distinct activation energies for melting and solidification so as to reduce thermal fluctuations at the interface. In order to allow the phase transition only at the interface we modify the switch functions in the following way:

$$K^{\pm}(\vec{r}_*, t_*) \to K^{\pm}(\vec{r}_*, t_*) \times \frac{1}{8} \sum \left\{ \frac{1}{2}[1 \pm \phi(\vec{r}_* + \vec{c}_i), t_*] \right\}^2. \quad (5)$$

Assuming $f_+ \equiv f_- = f$, $T_s = 0$, and $T'/T_w < 1$, a first order scale analysis leads to the partial differential

 0031-9007/01/86(16)/3578(4)$15.00

equation ($\phi_s = 1/2\{1 - \phi\}$):

$$\frac{\partial \phi_s}{\partial t} = f\phi_s(1 - \phi_s)(2\phi_s - 1) - f\phi_s(1 - \phi_s)\frac{T'}{T_w}. \tag{6}$$

This is the common phase-field equation (as, e.g., given by Beckermann *et al.* [10]) without the curvature term. From this we posit the relations $T_w = \Gamma/\delta$ and $f = \mu_k T_w/\delta$, where Γ is the Gibbs-Thomson coefficient, μ_k a kinetic coefficient, and δ the width of the transition region of the phase field. Latent heat release results in a change $\delta T_{\mathcal{L}} = -(\Delta T_*/\mathrm{St})(\delta\phi/2)$ of the temperature at node $\vec{r}_*$ and is added as a force term $F_i^{\mathcal{L}}$ in Eq. (1). $\mathrm{St} = c_p\Delta T/L$ is the Stefan number, ΔT_* and ΔT are the characteristic temperature differences of the system in lattice and physical units, c_p is the specific heat, and L is the latent heat. Latent heat is released in the solidification process ($\delta\phi < 0$) and absorbed in the melting process ($\delta\phi > 0$). The fluid-solid interaction is represented by an empirical mesoscopic drag force, $\vec{F}^{fs} = -\omega\vec{u}(1 - \phi)/2$, whose task is to enforce no flow in the solid phase. The relaxation parameter ω has been chosen of order 1 to assure that this relaxation is faster than any other process. The buoyancy force depends on the local phase field: $|\vec{F}^B| = \beta T(1 + \phi)/2$. The heat transfer over the interface is treated in the same way as in the single phases.

As all existing LB models with phase transitions, our scheme is empirical in character, hence potentially subject to high-Knudsen effects in the vicinity of thin interfaces. A detailed analysis of such subtle effects will be presented elsewhere; here we simply remark that use of separate populations for the phase field and temperature fields is likely to prove beneficial to numerical stability because it relieves a single discrete distribution function from the burden of fulfilling all the macroscopic constraints at a time.

A benchmark problem for numerical modeling of liquid-solid phase transition processes is the melting from a side of a Gallium rectangular layer developed by Gau and Viskanta, who studied the influence of melt convection on the phase boundary experimentally [11]. Since the first numerical simulation with a first-order finite volume enthalpy-porosity model in 1988 by Brent *et al.* [12], this has become a standard benchmark for liquid-solid phase transition modeling. Using a second order finite element approximation of an enthalpy-porosity model, Dantzig obtained a multicellular flow structure [13], whereas Brent *et al.* found a unicellular flow. From then on authors may be classified according to the computed melt flow structure, being either unicellular or multicellular [15]. Recently Cerimele *et al.* [16] proved that two possible sources of such a variety of physical and numerical configurations are poor space resolution of the numerical scheme and ambiguities in the description of the experiment [17]. These authors found a unicellular solution by a careful simulation

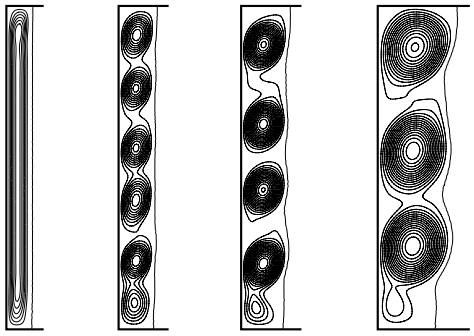

FIG. 1. Melting of Gallium: Results of the calculation at different times (from left to right: 20, 40, 60, and 120 s). Interfaces ($\phi = 0$) and streamlines are shown.

of the "pour-in/pour-out" technique used by the experimentalists to shot the phase interface: at each observed time instant they poured out the melt from the cavity, took the plot of the interface, then poured the melt in again and enhanced convection. This procedure was found to slow down the convection flow, thus preventing the formation of multiple cells.

Here we present a nonstop simulation of the Gau and Viskanta experiment. As expected, we obtain a multicellular melt flow. We start with a rectangular solid slab at melting temperature ($T = T_c$). The melting process starts when the temperature at the left wall is raised to $T_c + \Delta T_*$. Since the wall temperature is kept constant throughout the simulation, the melting front starts to propagate rightwards. Top and bottom walls are supposed adiabatic. Physical and geometrical parameters are taken from Gau and Viskanta's paper. The characteristic physical parameters of this test are the Rayleigh number $\mathrm{Ra} = 7 \times 10^5$, the Stefan number $\mathrm{St} = 0.0462$, and the Prandtl number $\mathrm{Pr} = 0.0216$. The simulation is run on a 400×560 grid over 6×10^4 time steps corresponding to 1 min

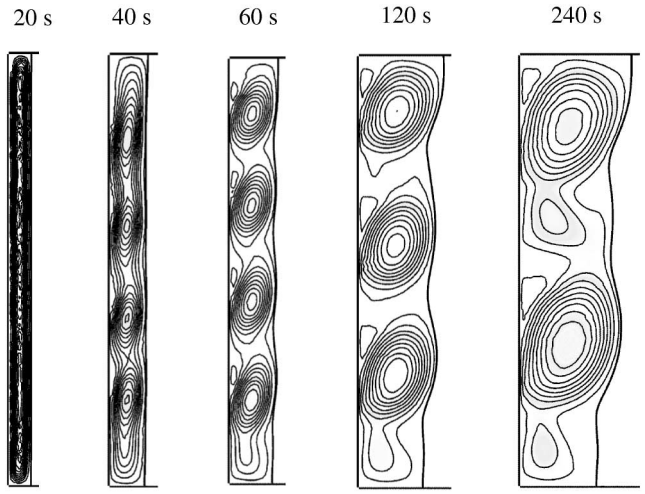

FIG. 2. Melting of Gallium: Results obtained by Wintruff [14] with an adaptive moving-grid method. Interfaces and streamlines at different times (from left to right: 20, 40, 60, and 120 s) are shown.

TABLE I. Parameters for the calculations of the crystal growth into an undercooled melt. ϵ_{diag} and ϵ_{vh} are the measures in diagonal and horizontal/vertical crystal directions, respectively.

$T_w \equiv T_s$	T_c	T_{init}	ΔT_*	$T_{\mathcal{L}}$	$f_+ \equiv f_-$	ϵ_{vh}	ϵ_{diag}
1×10^{-4}	0.0	-1×10^{-3}	1×10^{-3}	0.01	0.1	1.5	0.5

(physical time). The thermal diffusivity in lattice units is $D_* = 0.556$ and the frequency factors are $f_+ = f_- = 1 \times 10^{-3}$. This means that the ratio of chemical to diffusive time scales is approximately 10^{-3}, which is appropriate for the thin interface scenario relevant to this application. In Fig. 1, streamlines and interfaces ($\phi = 0$) are shown for different times. From this figure a reasonable agreement with a state-of-the-art computation on an adaptive grid (Fig. 2) is observed. The main quantitative discrepancy occurs at $t = 40$ s, where in the LB simulation still 6 separated rolls appear, whereas the calculation of Wintruff results in only 4 rolls. The discrepancies might be due to the general differences in the numerical methods and might be engendered by the extreme sensitivity of the flow structure in thin layers. In the LB method a transition (mushy) region exists, whereas in the other method the interface is sharp. By using the adaptive moving grid one cannot start with a fully solidified domain at $t = 0$ s, but has to start with a thin liquid layer. As time unfolds and the width of the slab increases, the differences in the flow pattern decrease. Our results are also qualitatively consistent with the computations by Dantzig [13] and by Gobin *et al.* [15]. The present LB code takes about 10 μs per grid point and time step on a midrange work station. This corresponds to about 1 d cpu per 1 min real time, which is of the same order as other existing methods need on a comparable work station [16].

As an example of crystal growth we discuss the solidification into an undercooled melt. In real applications the growth process is generally anisotropic. Anisotropy can be introduced into Eq. (5) by weighting the growth directions $0 \le \tilde{i} \le 1$. The directions $\tilde{i}$ for growth and i of the lattice *do not need to coincide,* but can form an angle $0 \le \alpha \le \pi/4 = a_\alpha \pi/4$. Let us consider the growth from a node $\vec{r}_*$. For every direction $\tilde{i}$ we compute

$$G_{\tilde{i}} = [\phi(\vec{r}_* + \vec{d}_{\tilde{i}}) - \phi(\vec{r}_* - \vec{d}_{\tilde{i}})][2 - |\phi(\vec{r}_* + \vec{d}_{\tilde{i}'}) - \phi(\vec{r}_* - \vec{d}_{\tilde{i}'})|] \times [2 - |\phi(\vec{r}_* + \vec{d}_{\tilde{i}'}) - \phi(\vec{r}_*)|][2 - |\phi(\vec{r}_* - \vec{d}_{\tilde{i}'}) - \phi(\vec{r}_*)|]; \quad (7)$$

$\tilde{i}'$ denotes the direction perpendicular to direction $\tilde{i}$ and $\vec{d}_{\tilde{i}}$ is a vector of unit length in direction $\tilde{i}$. The values at $\vec{r}_* + \vec{d}_{\tilde{i}}$ are computed by bilinear interpolation. We define a growth factor $\tilde{\phi}_{\tilde{i}}$ by

$$\tilde{\phi}_{\tilde{i}} = \begin{cases} \frac{2G_{\tilde{i}}}{\sum_{\tilde{i}} |G_{\tilde{i}}|}\{\frac{1}{2}[1 - \phi(\vec{r}_*)]\}^2 \epsilon_{\tilde{i}} & \text{if } G_{\tilde{i}} \ge 0\,, \\ \frac{2G_{\tilde{i}}}{\sum_{\tilde{i}} |G_{\tilde{i}}|}\{\frac{1}{2}[1 + \phi(\vec{r}_*)]\}^2 & \text{if } G_{\tilde{i}} < 0\,, \end{cases} \quad (8)$$

where $0 \le \epsilon_{\tilde{i}} \le 2$ is a measure of the anisotropy. We have to transform $\tilde{\phi}_{\tilde{i}}$ back on the lattice directions via $\tilde{\phi}_i = \{(1 - a_\alpha)\tilde{\phi}_{\tilde{i}} + a_\alpha \tilde{\phi}_{\tilde{i}-1}\} g_s$ where we count i in the same direction as the translation of i into $\tilde{i}$. The factor g_s recognizes if i is a diagonal direction ($g_s = 1/\sqrt{2}$) or a horizontal/vertical one ($g_s = 1$). Equation (5) modifies into

$$K^{\pm}(\vec{r}_*, t_*) \to K^{\pm}(\vec{r}_*, t_*) \times \frac{1}{8} \sum_i \max\{\mp \tilde{\phi}_i(\vec{r}_* - \vec{c}_i, t_*), 0\}. \quad (9)$$

Because of the definition in Eq. (7) a positive or negative $\tilde{\phi}$ means growth or solidification in this direction, respectively.

A series of runs has been performed for the growth of a circular seed with a radius of 3 lattice units (l.u.) into an undercooled melt in a box of 200×200 points. The general parameters are listed in Table I. The temperature at the boundary is fixed to 1×10^{-3} and nonslip boundary conditions are applied. As time proceeds, four branches develop (Fig. 3). We obtain a tip radius of 2.0 l.u. and a tip velocity 2.3×10^{-3} l.u. per iteration, which corresponds to a dimensionless radius ρ' of $200/\delta$ and a dimensionless tip velocity of $5 \times 10^{-5}\delta$, where 6δ is the width of the transition region ($-0.1 \le \phi \le 0.1$). δ is determined by a one-dimensional growth with the same parameters and has the value $\delta = 0.8$. Because ρ' is rather small we obtain different values for the undercooling from the modified Ivantsov and Temkin rule [18]: St = 0.05 (Ivantsov) and St = 0.09 (Temkin). The latter is in good agreement with the value of our calculation (St = 0.1). The growth of the dendrite can be enhanced by the buoyancy convection caused by the warm dendrite. We performed a calculation

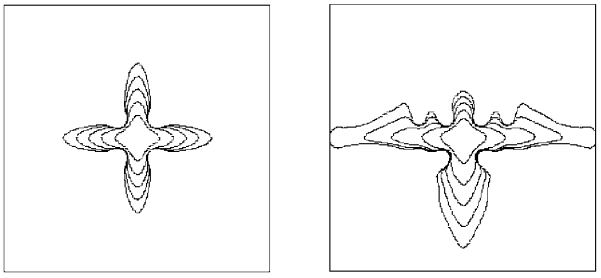

FIG. 3. Evolution of the isoline $\phi \equiv 0$ in time (4000, 8000, 12 000, 16 000, and 20 000 iterations) without (left) and with flow (right). The Rayleigh and Prandtl numbers are $\text{Ra} = 1.0 \times 10^5$ and $\text{Pr} = 0.1$, respectively. The crystal lattice corresponds with that for the hydrodynamic calculation.

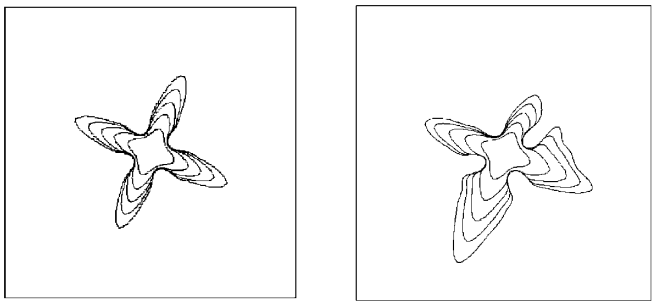

FIG. 4. Evolution of the isoline $\phi \equiv 0$ in time (4000, 8000, 12 000, 16 000, and 20 000 iterations) without (left) and with flow (right). The Rayleigh and Prandtl numbers are $\mathrm{Ra} = 1.0 \times 10^5$ and $\mathrm{Pr} = 0.1$, respectively. The crystal lattice is tilted by 18° against that for the hydrodynamic calculation.

for a Prandtl number $\mathrm{Pr} = 0.1$ and a Rayleigh number $\mathrm{Ra} = 1. \times 10^5$, where the latter is defined via $\mathrm{Ra} = \beta \Delta T_* N^3/(\nu_* D_*)$ (N: number of grid points in x direction). The four convection rolls near the dendrite interface provide an efficient convective heat transport so that the two side arms can grow fast (Fig. 3, right and Fig. 5, left). In the next run we tilt the crystal lattice by 18° against the underlying lattice for the hydrodynamic calculation. For zero flow we obtain the same result as in the untilted case (Fig. 4, left). In the case with buoyancy convection different flow and dendrite structure is observed for the untilted and the tilted case (Fig. 5).

We wish to emphasize that the basic assets of the LB method, namely simplicity and outstanding amenability to parallel computing, are fully retained in spite of the significant complexity of solidification/melting phenomena.

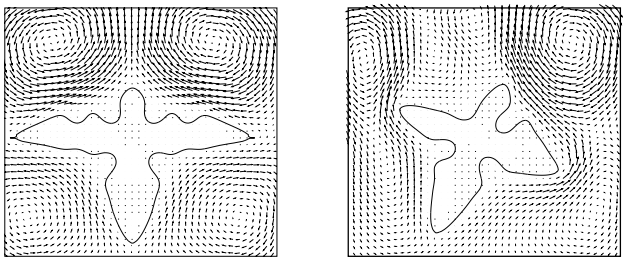

FIG. 5. Velocity field around the dendrite for the untilted (left) and the tilted crystal lattice (right) after 15 000 iterations. The Rayleigh and Prandtl numbers are $\mathrm{Ra} = 1.0 \times 10^5$ and $\mathrm{Pr} = 0.1$, respectively.

Financial support from ESF-PESC Scientific Programme "Challenges in molecular simulations: bridging the length and time scale gap" is kindly acknowledged. W. M. and S. S. wish to thank Professor M. Mareschal for enlightening discussion and kind hospitality at CECAM. W. M. gratefully thanks I. Wintruff for fruitful discussions and for providing Fig. 2.

*Electronic address: wm@ikz-berlin.de

[1] S. Chen and G. Doolen, Annu. Rev. Fluid Mech. **30**, 329 (1998).
[2] G. de Fabritiis, A. Mancini, D. Mansutti, and S. Succi, Int. J. Mod. Phys. C **9**, 1405 (1998).
[3] F. Higuera, S. Succi, and R. Benzi, Europhys. Lett. **9**, 345 (1989).
[4] R. Benzi, S. Succi, and M. Vergassola, Phys. Rep. **222**, 145 (1992).
[5] A. Calì, S. Succi, A. Cancelliere, R. Benzi, and M. Gramignani, Phys. Rev. A **45**, 5771 (1992).
[6] W. Miller and K. Böttcher, Int. J. Mod. Phys. C **9**, 1567 (1998).
[7] F. Massaioli, S. Succi, and R. Benzi, Europhys. Lett. **21**, 305 (1993).
[8] F. Massaioli, R. Benzi, S. Succi, and R. Tripiccione, Europ. J. Fluid Mech. **14**, 1 (1995).
[9] W. Miller, Phys. Rev. E **51**, 3659 (1995).
[10] C. Beckermann, H.-J. Diepers, I. Steinbach, A. Karma, and X. Tong, J. Comput. Phys. **154**, 468 (1999).
[11] C. Gau and R. Viskanta, J. Heat Transfer **108**, 174 (1986).
[12] A. D. Brent, V. R. Voller, and K. Reid, Numer. Heat Transfer **13**, 297 (1988).
[13] J. A. Dantzig, Int. J. Numer. Methods Eng. **28**, 1769 (1989).
[14] I. Wintruff, Ph.D. thesis, Universität Karlsruhe, 2000.
[15] D. Gobin and P. L. Quéré, Comput. Assist. Mechan. Eng. Sci. **7**, 289 (2000).
[16] M. M. Cerimele, D. Mansutti, and F. Pistella, in State of the Art in CFD, Proceeding of the Conference to Honour R. Peyret on His 60th Birthday, Marseille, 1999 [Comput. Fluids (to be published)].
[17] M. M. Cerimele, D. Mansutti, and F. Pistella, in *CD-ROM Proceedings of E.C.C.O.M.A.S. 2000* (CIMNE, Barcelona, 2000).
[18] J. S. Langer, Rev. Mod. Phys. **52**, 1 (1980).